Effect of Ga Content on the Instantaneous Structure of $Al_{(1-x)}Ga_xPO_4$ Solid Solutions at High Temperature

Olivier Cambon,* Julien Haines, and Martine Cambon

Institut Charles Gerhardt Montpellier, UMR-CNRS-UM2-ENSCM-UM1 5253, Université Montpellier 2, Equipe PMOF, Place E.Bataillon, 34095 Montpellier, Cedex 5, France

David A. Keen, Matthew G. Tucker, and Laurent Chapon

ISIS Facility, Rutherford Appleton Laboratory, Harwell Science and Innovation Campus, Didcot, Oxfordshire OX11 0QX, United Kingdom

Niels K. Hansen,† Mohamed Souhassou, and Florence Porcher

LCM3B, UMR-CNRS 7036, Nancy Université, 54506 Vandoeuvre-lès-Nancy, France

Received June 18, 2008. Revised Manuscript Received November 25, 2008

$Al_{(1-x)}Ga_xPO_4$ solid solutions (x= 0.14, 0.2, and 0.63) were studied at high temperature up to 1173 K by neutron total scattering. Rietveld refinements confirm the presence of the β-quartz-type structure for the lowest Ga content. On the basis of the refinement of the average structure at high temperature, the Al−O and Ga−O distances cannot be distinguished and all intratetrahedral bond distances decrease, which is not reasonable when compared to the thermal expansion behavior of this material. This apparent behavior is due to the presence of a high degree of dynamic disorder at high temperature. In contrast, reverse Monte Carlo (RMC) modeling of neutron total scattering data gives the instantaneous structure in which the two bonds (Al−O) at ∼1.75 Å and (Ga−O) at ∼1.84 Å are partially resolved and increase in length with temperature. The Ga content of the solid solutions is found to modify the structural geometry at high temperature. Increasing the Ga content reduces the Al−O−P angles compared to pure $AlPO_4$ and lessens their temperature dependence. The results also show that the dynamic disorder in the oxygen sublattice decreases with the Ga-content. As in quartz, the displacive α−β phase transition (for x = 0.14) can be linked to cation displacements as the oxygen sublattice presents a high degree of dynamic disorder well below the transition temperature. The increased temperature stability for Ga-rich compositions can be linked to stronger covalent bonding as is found from the analysis of electron density maps of the pure $AlPO_4$ and $GaPO_4$ end members. This approach, based on using chemical substitution to reinforce the covalent nature of chemical bonds, may have implications for improving the thermal stability of a variety of materials used in high-temperature applications.

1. Introduction

Quartz has a great importance in electronics due to its piezoelectric properties. However, the performance of quartz is insufficient for certain applications that require a high thermal stability or a high electro-mechanical coupling coefficient. The structures of quartz homeotypes $A^{III}B^{V}O_4$ (A^{III} = B, Al, Ga, Fe and B^{V}= P, As) belong to space groups $P3_121$ or $P3_221$ with $Z = 3$ and the structure can be described as a helicoidal chain of tetrahedra along the z-axis with alternating AO_4 and BO_4 tetrahedra. Important structure−property relationships have been established in these materials between thermal stability, physical and piezoelectric properties and the structural distortion with respect to the β-quartz structure type.[1−10] This distortion is quantified by the intertetrahedral bridging θ angle (Figure 1) and the tetrahedral tilt angle (δ),[11] which is the order parameter for the α−β transition and corresponds to the rotation of the tetrahedra about their 2-fold axes parallel to x. For α-quartz at room temperature, $\theta = 143.6°$, $\delta = 16.4°$ and for β-quartz at 848 K, $\theta = 153.3°$, $\delta = 0°$.[12] There is a linear dependence between the electromechanical coupling coefficient and the

* Corresponding author. E-mail: ocambon@lpmc.univ-montp2.fr.
† In memoriam.

(1) Philippot, E.; Goiffon, A.; Ibanez, A.; Pintard, M. *J. Solid State Chem.* **1994**, *110*, 356.
(2) Philippot, E.; Palmier, D.; Pintard, M.; Goiffon, A. *J. Solid State Chem.* **1996**, *123*, 1.
(3) Philippot, E.; Armand, P.; Yot, P.; Cambon, O.; Goiffon, A.; McIntyre, G. J.; Bordet, P. *J. Solid State Chem.* **1999**, *146*, 114.
(4) Haines, J.; Chateau, C.; Léger, J. M.; Marchand, R. *Ann. Chim. Sci. Mater.* **2001**, *26*, 209.
(5) Haines, J.; Cambon, O.; Philippot, E.; Chapon, L.; Hull, S. *J. Solid State Chem.* **2002**, *166*, 434.
(6) Haines, J.; Cambon, O.; Hull, S. *Z. Kristallogr.* **2003**, *218*, 193.
(7) Cambon, O.; Yot, P.; Rul, S.; Haines, J.; Philippot, E. *Solid State Sci.* **2003**, *5*, 469.
(8) Cambon, O.; Haines, J. *Proceedings of the 2003 IEEE International Frequency Control Symposium & 17th European Frequency and Time Forum*; Tampa, FL, May 8, 2003; IEEE: Piscataway, NJ, 2003; p 650.
(9) Haines, J.; Cambon, O.; Astier, R.; Fertey, P.; Chateau, C. *Z. Kristallogr.* **2004**, *219*, 32.
(10) Haines, J.; Cambon, O. *Z. Kristallogr.* **2004**, *219*, 314.
(11) Grimm, H.; Dorner, B. *J. Phys. Chem. Solids* **1975**, *36*, 413.
(12) Kihara, K. *Eur. J. Mineral.* **1990**, *2*, 63.

10.1021/cm801667p CCC: $40.75
Published on Web 12/24/2008

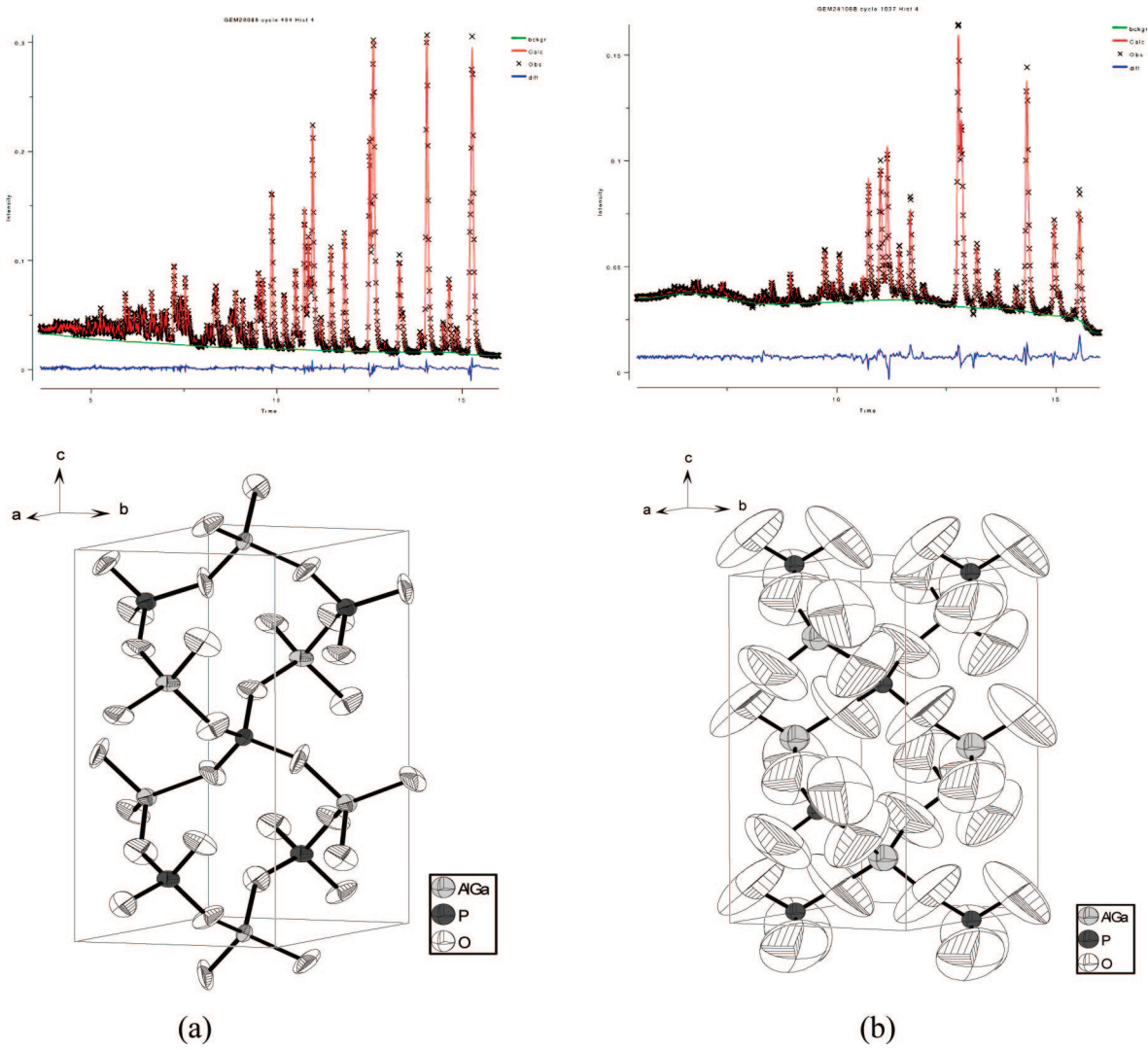

Figure 1. Rietveld refinements using neutron powder diffraction patterns and crystal structure of $Al_{0.86}Ga_{0.14}PO_4$ at (a) room temperature (α-quartz: $P3_121$) and (b) 1018 K (β-quartz: $P6_422$). The ellipsoids are represented at the 99% probability level.

structural distortion; $GaAsO_4$ has been found to be the most distorted and has the highest electromechanical coupling coefficient ($k = 21\%$) in the quartz group.[13] This coupling coefficient corresponds to the efficiency of the conversion between mechanical and electric energy. From resonator measurements, this coefficient is given by

$$k = \pi/2[(f_a - f_r)/f_a]^{1/2}$$

where f_r and f_a are the frequencies of resonance and antiresonance, respectively.

Moreover, $GaAsO_4$ does not present an α-β phase transition and its α-phase structure is stable up to thermal decomposition at 1300 K. To determine the influence of the structural distortion upon piezoelectric properties and thermal stability more accurately, a study of the $AlPO_4-GaPO_4$ system has been undertaken. Solid solutions are of particular interest as chemical composition can be used to tune the piezoelectric properties of crystals.[14] The two end members of this system present different high temperature behavior. $AlPO_4$ is less distorted ($\theta = 142.5°$, $\delta = 17.6°$, and $k = 11\%$) and exhibits a displacive α−β phase transition, whereas $GaPO_4$ is more distorted ($\theta = 134.6°$, $\delta = 23.3°$, and $k = 16\%$) and a direct reconstructive phase transition from an α-quartz to a β-cristobalite form occurs. Among α-quartz homeotypes several solid solutions have already been studied (SiO_2-GeO_2,[15,16] SiO_2-PON,[4] SiO_2-AlPO_4,[17] $AlPO_4-GaPO_4$,[14,18−20] $AlPO_4-AlAsO_4$,[18] $AlPO_4-FePO_4$[21]). In particular, for the $Al_{(1-x)}Ga_xPO_4$ system it was demonstrated that[14] the structural distortion (i.e., θ and δ) varies quite

(13) Cambon, O.; Haines, J.; Fraysse, G.; Détaint, J.; Capelle, B.; Van der Lee, A. *J. Appl. Phys.* **2005**, *97*, 074110.
(14) Haines, J.; Cambon, O.; Cachau-Herreillat, D.; Fraysse, G.; Mallassagne, F. E. *Solid State Sci.* **2004**, *6*, 995.
(15) Miller, W S.; Dachille, F.; Shafer, E. C.; Roy, R. *Am. Mineral.* **1963**, *48*, 1024.
(16) Fursenko, B. A.; Kirkinsky, V. A.; Rjaposov, A. P. High-Pressure Science and Technology Proceedings of the 7th AIRAPT International Conference; Vodar, B., Marteau, P., Eds.; Pergamon: Oxford, U.K., 1980; p 562.
(17) Veksler, I. V.; Thomas, R.; Wirth, R. *Am. Mineral.* **2003**, *88*, 1724.
(18) Cachau-Herreillat, D.; Bennazha, J.; Goiffon, A.; Ibanez, A.; Philippot, E. *Eur. J. Solid State Inorg. Chem.* **1992**, *29*, 1295.
(19) Xia, H. R.; Qin, Z. K.; Yuan, W.; Liu, S. F.; Zou, Z. Q.; Han, J. R. *Cryst. Res. Technol.* **1997**, *32*, 783.
(20) Barz, R. U.; David, F.; Schneider, J.; Gille, P. *Z. Kristallogr.* **2001**, *216*, 501.
(21) Mohamed, F. Sh. *Adsorpt. Sci. Technol.* **2002**, *20*, 741.

linearly as a function of x. This may open the way to tune the piezoelectric properties of crystals in this system by varying the composition. Similarly, the thermal stability with respect to the β-quartz structure type will vary as a function of initial structural distortion by changing composition. There are, however, other phase transitions which intervene at high temperature, in particular, reconstructive transitions to tridymite or β-cristobalite forms.[18,20,22,23] $Al_{1-x}Ga_xPO_4$ solid solutions with the α-quartz-type structure have been investigated up to 1208 K by X-ray powder diffraction.[24] The α-β quartz transition is not observed for the Ga-rich compositions and only the transition to the β-cristobalite form occurs. A phase diagram was proposed for the $AlPO_4-GaPO_4$ system. These results fix a limit for the presence of the α−β transition in the α-quartz type materials: no α−β quartz transition occurs for $\theta < 141°$ and $\delta > 18.5°$. An exception to this is $FePO_4$, which presents an α−β quartz transition although it is highly distorted at room temperature ($\theta = 137.8°$ and $\delta = 21.5°$).[6] This behavior has been attributed to the presence of 3d electrons of the Fe^{3+} cations.

High-temperature dynamic disorder in quartz SiO_2[25] has been studied by total neutron scattering. The instantaneous structure at high-temperature has been determined using reverse Monte Carlo modeling. In this work, the displacive α−β quartz transition was described in detail. It was shown that the classical soft-mode picture of the phase transition at $T_c = 846$ K is too simplistic. In addition to the phase transition, the authors demonstrated that important thermally induced structural disorder appears well before the classical T_c. More recently,[26,27] piezoelectric measurements at high temperature on quartz resonators have been coupled to these neutron total scattering results. The quality Q-factor of the resonators decreases dramatically beginning above 573 K and well below T_c. This behavior has been attributed to the instantaneous local disorder in the oxygen sublattice, which dissipates the induced dipoles and consequently decreases the Q-factor. A similar study of dynamic disorder has been performed on $GaPO_4$[28] which does not exhibit a β-quartz phase. Gallium orthophosphate was studied at high temperature up to 1303 K by neutron total scattering and to 1173 K by piezoelectric measurements. Reverse Monte-Carlo (RMC) refinements of the neutron total scattering data indicated that although the degree of structural disorder initially varies only slowly over a very large temperature interval in the α-quartz-type phase, an increase in disorder is observed beginning above 1023 K. Piezoelectric measurements indicated that the quality factor (Q) of $GaPO_4$ resonators remains stable up to this temperature but above this the piezoelectric properties of the material degrade. This degradation can also be correlated to the increase in structural disorder. By comparing SiO_2 and $GaPO_4$, total neutron scattering studies show that in quartz, which undergoes an α−β quartz transition, the disorder increases much faster as a function of temperature than in $GaPO_4$, which does not exhibit an α−β quartz transition. A high temperature Raman scattering study of $GaPO_4$ and $Al_{1-x}Ga_xPO_4$[29] has shown that the broadening of the decoupled GaO_4 tetrahedral libration mode increases more rapidly in the Al-rich compositions. Decoupled modes correspond to modes that are linked to either AlO_4 or GaO_4 tetrahedra and do not appear in the spectrum of the opposite end member.[29] Their frequencies vary little with chemical composition. These results indicate that dynamic disorder may appear at lower temperatures for Al-rich compositions in the solid solutions for which the β-quartz phase is observed. The present high-temperature neutron total scattering study of $Al_{1-x}Ga_xPO_4$ was performed to better understand the influence of chemical composition on the dynamic disorder in these materials and to predict its effect on piezoelectric properties.

2. Experimental Section

2.1. Synthesis of $Al_{1-x}Ga_xPO_4$ Powders. The powders were prepared by hydrothermal methods.[18,24,29] Solutions of $GaPO_4$ and $AlPO_4$ in sulfuric acid were prepared separately. Suitable quantities of these solutions are then mixed, taking into account the differences in solubility of the two end members, and placed into a PTFE-lined autoclave, which was heated in order to induce crystallization of the solid solution. The compositions of the powder samples were determined from the *c/a* cell parameter ratio obtained by X-ray powder diffraction measurements performed on a PANanalytical X'Pert diffractometer equipped with an X'Celerator detector using Ni-filtered, Cu Kα radiation.[24] In this paper, the three compositions studied were $x = 0.14$, 0.2, and 0.63.

2.2. High-Temperature Total Neutron Scattering.

2.2.1. Data Acquisition. This study was performed on the GEM time-of- flight (TOF) neutron diffractometer at the ISIS spallation source of the Rutherford Appleton Laboratory (RAL). For each composition, 4 g of powder were placed in an 8 mm diameter cylindrical vanadium can. The sample was then placed inside a furnace and heated from RT up to 1173 K. Scattering from the sample was collected using several banks of ZnS scintillator detectors, covering scattering angles 2θ from 6 to 149° and using a time-of-flight range from 0.8 to 20 ms. This corresponds to an approximate range of scattering vectors, Q, between 0.1 and 50 $Å^{-1}$. To obtain very good statistics, particularly in the important high-Q region, data were collected for 6 hours at each temperature. The instrument was calibrated using measurements of a vanadium rod, the empty furnace and an empty can in the furnace to take into account all the scattering contributions of the sample environment and to normalize the data on an absolute scale. In parallel with these corrections, the data were normalized and corrected for absorption to produce powder patterns for Rietveld structure refinements.

2.2.2. Rietveld Refinements. The average structure of the samples at each temperature were refined using the program GSAS[30] using the data from detector banks 3 (centered on $2\theta = 35°$; $d = 1-5$ Å), 4 (centered on $2\theta = 63.6°$; $d = 0.7-3.714$ Å), 5 (centered on

(22) Achary, S. N.; Jayakumar, O. D.; Tyagi, A. K.; Kulshresththa, S. K. *J. Solid State Chem.* **2003**, *176*, 37.
(23) Flörke, O. W. *Z. Kristallogr.* **1967**, *125*, 134.
(24) Haines, J.; Cambon, O.; Fraysse, G.; Van der Lee, A. *J. Phys.: Condens. Matter* **2005**, *17*, 4463–4474.
(25) Tucker, M. G.; Keen, D. A.; Dove, M. T. *Mineral. Mag.* **2001**, *65*, 489.
(26) Haines, J.; Cambon, O.; Keen, D. A.; Tucker, M. G.; Dove, M. T. *Appl. Phys. Lett.* **2002**, *81*, 2968.
(27) Haines, J.; Cambon, O.; Keen, D. A. *Physica B* **2004**, 350.
(28) Haines, J.; Cambon, O.; Prud'homme, N.; Fraysse, G.; Keen, D. A.; Chapon, L. C.; Tucker, M. G. *Phys. Rev. B* **2006**, *73*, 014103.
(29) Angot, E.; Le Parc, R.; Levelut, C.; Beaurain, M.; Armand, P.; Cambon, O.; Haines, J. *J. Phys.: Condens. Matter* **2006**, *18*, 4315–4327.
(30) Larson, A. C.; Von Dreele, R. B. *GSAS: General Structure Analysis System*; Los Alamos National Laboratory: Los Alamos, NM, 1994.

$2\theta = 91.3°$; $d = 0.5-2.385$ Å) and 6 (centered on $2\theta = 154.4°$; $d = 0.5-1.765$ Å). The cell constants, atomic positions, anisotropic atomic displacement parameters, scale factor, and two line shape parameters were varied in the refinements, along with up to 25 background parameters to account for background contributions due to diffuse scattering. No restraint was used. The χ^2 values are higher than usual because of the long data acquisition time needed for the total scattering analysis.

2.2.3. Pair Distribution Functions (PDF). Normalized total scattering data were collected from the different GEM detector banks and combined together to obtain the total scattering factor, $F(Q)$, for each temperature. The normalization procedure was carried out using the GUDRUN program, which is based on the ATLAS analysis package.[31] Then a Fourier Transform of $F(Q)$ was performed to obtain the distribution $G(r)$ in terms of the atomic distance r. G(r) is a sum of all the atomic partial pair distances and contains information about the number of atoms of type i around an atom of type j, averaged over all the j atoms.[32]

2.2.4. RMC Modeling. Reverse Monte Carlo modeling,[33] as incorporated within the program RMCProfile,[34] was used to obtain bond and bond angle distributions and the overall topology of the instantaneous structure. Here, the first step consists of the creation of an ($8 \times 8 \times 4$) supercell of the average unit cell. The atoms are randomly moved and $F(Q)$, $G(r)$, and diffraction patterns are computed from the supercell. The comparison of the computed and the experimental data is used to accept or reject the random moves until the supercell model yields $F(Q)$, $G(r)$, and Bragg diffraction patterns in good agreement with the experimental data. This instantaneous representation of the structure can be used to calculate correlation functions which provide important additional information with respect to the average structure determined from Rietveld refinement.

2.3. $AlPO_4$ and $GaPO_4$ Single-Crystal High-Resolution XRD. $AlPO_4$[35,36] and $GaPO_4$[37] single crystals were grown by hydrothermal methods.

2.3.1. Data Acquisition. High-resolution single-crystal X-ray diffraction experiments were performed at 110 K with a Nonius Kappa CCD diffractometer (Mo(Kα) radiation, $\lambda = 0.709$Å). A complete and redundant data set was measured up to $(\sin\theta/\lambda)_{max} \approx 1.2$ Å^{-1}. Bragg intensities were integrated with the HKL2000 program package[38] and corrected from absorption[39] before scaling and averaging.[40,41]

2.3.2. Electron Density Analysis. The electron density ρ was modeled according to the Hansen-Coppens multipolar formalism[42] and refined by least-squares against experimental structure factors moduli. Isotropic extinction was corrected according to the Becker−Coppens formula[43] and was marked for $GaPO_4$ ($\eta = 0.17$). The quality of the fit was assessed by the agreement factors ($AlPO_4$: $R = 1.39\%$ $R_w = 1.64\%$ GOF = 0.45; $GaPO_4$: R = 3.8%, $R_w = 5.3\%$ GOF = 1.04), and overall by inspection of $\Delta\rho$ dynamic deformation density maps

$$\Delta\rho_{dyn}(\vec{r}) = \frac{1}{V}\sum_{\vec{H}}\left(\frac{1}{k}|F_{mul}(\vec{H})|e^{i\phi_{mul}} - |F_{sph}(\vec{H})|e^{i\phi_{sph}}\right)e^{i2\pi\vec{H}\cdot\vec{r}}$$

calculated using F_{sph}/F_{mul} structure factors evaluated, respectively, using spherical free-atom form factors or form factors derived form multipolar modeling, and taking into account harmonic thermal displacement. Atomic charges were estimated by a topological analysis of the electron density[44] using the program Newprop.[45]

Table 1. Unit-Cell Parameters, Volume, and Agreement Factors for the Different Compositions of $Al_{(1-x)}Ga_xPO_4$ as a Function of Temperature (β-Quartz Structure for $x = 0.14$ at 1018 K)

T(K)	a(Å)	c(Å)	V(Å^3)	R_{wp}	R_p	χ^2
		$Al_{0.86}Ga_{0.14}PO_4$				
290	4.93725(2)	10.95723(7)	231.314(3)	0.0311	0.0315	12.17
873	5.00236(5)	11.03132(16)	239.061(8)	0.0373	0.0342	12.79
1018	5.04155(6)	11.06965(21)	243.665(10)	0.0406	0.0352	14.92
		$Al_{0.8}Ga_{0.2}PO_4$				
290	4.93171(2)	10.95423(7)	230.732(3)	0.0296	0.0315	10.83
473	4.94612(3)	10.96969(8)	232.410(4)	0.0287	0.0302	9.62
573	4.95528(3)	10.98000(8)	233.491(5)	0.0283	0.0306	7.57
633	4.96136(3)	10.98676(8)	234.208(5)	0.0285	0.0297	7.38
693	4.96794(2)	10.99437(9)	234.993(2)	0.0468	0.0442	13.07
783	4.97896(3)	11.00645(10)	236.295(5)	0.0290	0.0303	7.41
873	4.99233(4)	11.02127(11)	237.886(6)	0.0297	0.0299	7.74
		$Al_{0.37}Ga_{0.63}PO_4$				
290	4.91799(2)	11.00621(8)	230.539(4)	0.0333	0.0317	12.37
473	4.9272(2)	110111(5)	231.51(2)	0.0308	0.0310	9.32
673	4.94515(3)	11.03098(9)	233.617(5)	0.0339	0.0330	10.08
873	4.96399(3)	11.04917(11)	235.788(5)	0.0413	0.0366	11.56

3. Results and Discussion

3.1. Average Structures−Rietveld Refinements of Powder Neutron Diffraction. Rietveld refinements (Tables 1 and 2, panels a and b in Figure 1) confirm the high-temperature structural evolution previously determined by X-ray diffraction[24] with, in the present case, significantly lower esd's on the fractional coordinates of the oxygen atoms and more accurate atomic displacement parameters (ADP). The β-quartz-type structure was observed for the lowest Ga-content at 1018K. As in previous X-ray diffraction studies, there was no evidence for Al/Ga ordering; Rietveld refinements were performed with the Al and Ga atoms randomly occupying 3*a* sites with an average fractional occupation $1-x$ and x, respectively. The Rietveld data—particularly the atomic displacement parameters—give important information about the disorder at high temperature. At 873 K, the atomic displacement parameters of the cations depend little on the composition x_{Ga}; 5% and 1% relative variation of the values for the Al/Ga and P cations are observed respectively from samples with $x = 0.14$ to $x = 0.63$. In contrast, the atomic displacement parameters of the oxygen atoms are twice that of cations and the relative variation decreases by 20% with increasing Ga-content. These results indicate that a higher

(31) Hannon, A. C.; Howells, W. S.; Soper, A. K. *Inst. Phys. Conf. Ser.* **1990**, *107*, 193.
(32) Keen, D. A. *J. Appl. Crystallogr.* **2001**, *34*, 172.
(33) McGreevy, R. L. *J. Phys.: Condens. Matter* **2001**, *13*, R877.
(34) Tucker, M. G.; Keen, D. A.; Dove, M. T.; Goodwin, A. L.; Hui, Q. *J. Phys.: Condens. Matter* **2007**, *19*, 335218.
(35) Jumas, J. C.; Goiffon, A.; Capelle, B.; Zarka, A.; Doukhan, J. C.; Schwartzel, J.; Détaint, J.; Philippot, E. *J. Cryst. Growth* **1987**, *80*, 133.
(36) Cambon, O.; Goiffon, A.; Philippot, E. *J. Solid State Chem.* **1989**, *78*, 187.
(37) Cambon, O.; Yot, P.; Balitsky, D.; Goiffon, A.; Philippot, E.; Capelle, B.; Détaint, J. *Ann. Chim. Sci. Mater.* **2001**, *26*, 79.
(38) Otwinowski, Z.; Minor, W.; Raynor, J.; Henderson, K.; Majewski, W.; Mohanty, N.; Cymborowski, M. *HKL2000*; HKL Research: Charlottesville, VA, 2000.
(39) DeTitta, G. T. *J. Appl. Crystallogr.* **1985**, *18*, 75.
(40) Blessing, R. H. *J. Appl. Crystallogr.* **1997**, *30*, 421.
(41) Blessing, R. H.; Guo, D. Y.; Langs, D. A. Intensity Statistics and Normalization. In *Direct Methods for Solving Macromolecular Structures*; Fortier, S., Ed.; Kluwer Academic: Dordrecht, The Netherlands, 1998; Vol. 47. and references therein.
(42) Hansen, N. K.; Coppens, P. *Acta Crystallogr., Sect. A* **1978**, *A34*, 909.
(43) Becker, P. J.; Coppens, P. *Acta Crystallogr., Sect. A* **1974**, *30*, 129.
(44) Bader, R. F. Atoms in Molecules: A Quantum Theory; Clarendon Press: Oxford, U.K., 1990.
(45) Souhassou, M.; Blessing, R. H. *J. Appl. Crystallogr.* **1999**, *32*, 210.

Table 2. Fractional Atomic Coordinate and Thermal Atomic Displacement Parameters (Å^2) for the Different Compositions of $Al_{(1-x)}Ga_xPO_4$ as a Function of Temperature[a]

T(K)	$x_{(Al,Ga)}$	100 × (U_{iso} or U_{eq})[b]	x_P	100 × (U_{iso} or U_{eq})[b]	x_{O1}	y_{O1}	z_{O1}	100 × U_{eq}	x_{O2}	y_{O2}	z_{O2}	100 × U_{eq}
					$Al_{0.86}Ga_{0.14}PO_4$							
290	0.4650(4)	0.53(5)*	0.4660(2)	0.52(3)*	0.4160(2)	0.2960(1)	0.39692(4)	1.09(3)	0.4142(2)	0.2601(1)	0.88183(5)	1.15(3)
873	0.4796(5)	1.85(6)	0.4718(4)	2.08(4)	0.4216(4)	0.2788(3)	0.40436(9)	4.8(1)	0.4173(4)	0.2408(2)	0.89064(9)	4.9(1)
1018[c]	0.5000	2.96(6)	0.5000	3.29(5)	0.4191(1)	0.2271(2)	0.58978(8)	7.75(7)				
					$Al_{0.8}Ga_{0.2}PO_4$							
290	0.4627(2)	0.54(2)	0.4650(2)	0.66(2)	0.4149(2)	0.2975(1)	0.39656(4)	1.22(2)	0.4137(2)	0.2606(1)	0.88110(4)	1.19(3)
473	0.4645(3)	0.87(2)	0.4675(3)	1.09(2)	0.4154(2)	0.2937(1)	0.39786(5)	2.01(4)	0.4151(2)	0.2575(1)	0.88259(5)	1.92(3)
573	0.4651(3)	1.13(2)	0.4694(2)	1.24(2)	0.4159(2)	0.2912(2)	0.39878(5)	2.54(4)	0.4157(2)	0.2551(1)	0.88350(5)	2.40(4)
633	0.4661(3)	1.31(3)	0.4705(3)	1.37(2)	0.4162(2)	0.2895(2)	0.39941(5)	2.86(5)	0.4162(2)	0.2536(2)	0.88417(5)	2.70(5)
693	0.4665(4)	1.42(4)	0.4716(4)	1.57(3)	0.4163(3)	0.2876(2)	0.40013(7)	3.25(7)	0.4168(3)	0.2524(2)	0.88490(7)	3.05(7)
783	0.4684(4)	1.66(4)	0.4740(4)	1.83(3)	0.4166(3)	0.2842(2)	0.40151(6)	3.77(7)	0.4178(3)	0.2493(2)	0.88621(7)	3.65(7)
873	0.4710(5)	1.85(4)	0.4762(4)	2.05(3)	0.4172(3)	0.2797(3)	0.40336(7)	4.52(8)	0.4190(3)	0.2448(2)	0.88818(8)	4.48(8)
					$Al_{0.37}Ga_{0.63}PO_4$							
290	0.4593(2)	0.63(4)*	0.4610(2)	0.60(4)*	0.4122(2)	0.3086(1)	0.39431(4)	1.22(3)	0.4112(2)	0.2664(2)	0.87612(6)	1.36(4)
473	0.4612(2)	0.96(4)*	0.4616(2)	0.92(5)*	0.4128(2)	0.3063(1)	0.39511(5)	1.87(4)	0.4120(2)	0.2635(2)	0.87729(6)	1.91(4)
673	0.4635(3)	1.39(5)*	0.4630(3)	1.47(6)*	0.4134(3)	0.3027(2)	0.39637(6)	2.96(5)	0.4140(3)	0.2609(2)	0.87877(8)	2.89(6)
873	0.4651(3)	1.74(3)	0.4667(4)	2.06(4)	0.4143(3)	0.2988(3)	0.39783(8)	4.19(7)	0.4140(4)	0.2565(3)	0.88076(10)	3.89(8)

[a] For the α-quartz structured phase, (Al,Ga) are placed in 3*a* (*x*,0,1/3) sites, P are in 3*b* (*x*,0,5/6) sites, and O1 and O2 are both in 6*c* (*x*,*y*,*z*) sites of space group $P3_121$. Atoms in the *β*-quartz structured phase are placed with (Al,Ga) in 3*d* (1/2,0,1/2), P in 3*c* (1/2,0,0), and O in 12*k* (*x*,*y*,*z*) in space group $P6_422$; there is a change in origin of +(0,0,1/6) from the α-quartz setting. [b] Asterisk indicates U_{eq} value; all other values are for U_{iso}. [c] *β*-quartz structure.

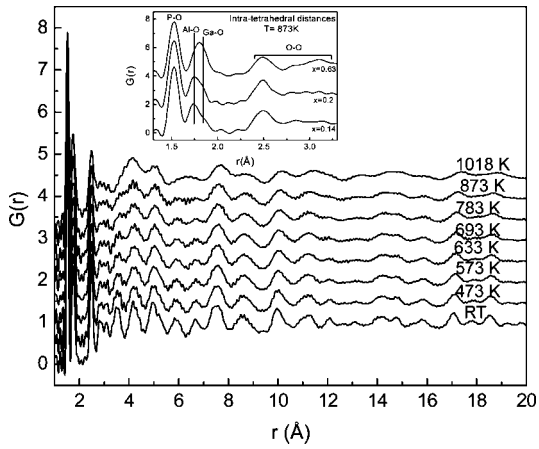

Figure 2. Pair distribution functions $G(r)$ in terms of atomic distances for x_{Ga}= 0.2 at each temperature (for T= 1018 K, x_{Ga}= 0.14). Peaks corresponding to the intratetrahedral distances at 873 K for x = 0.14, 0.2, and 0.63 are shown in the inset.

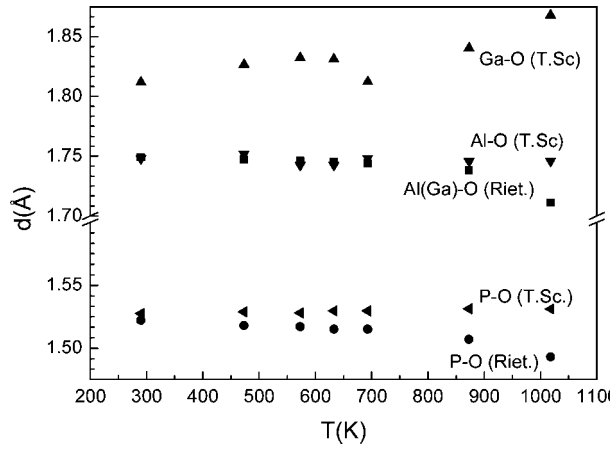

Figure 3. Intratetrahedral interatomic distances obtained by Rietveld refinements (Riet.) and by total scattering (T.Sc.) as a function of temperature for x_{Ga}= 0.2 at each temperature (for T = 1018 K, x_{Ga}= 0.14).

degree of disorder is present in the oxygen sublattice for higher Al contents.

3.2. Instantaneous Structure−Pair Distribution Functions. Bond lengths were directly determined from the pair distribution functions $G(r)$ obtained from the total neutron scattering factors $F(Q)$ at each temperature (Figure 2). Each peak in $G(r)$ corresponds to a bond length between two atoms in the structure. The intratetrahedral bonds correspond to the distances up to ∼3.0 Å, where the shortest peak (about 1.55 Å) is the P−O bond and the second peak (from 1.7 to 1.9 Å) contains the Al−O and Ga−O bonds. This second peak is particularly interesting. In fact, this peak can be separated into two components corresponding to the Al−O bond at about 1.75 Å and Ga−O bond at about 1.84 Å. The peak centered at ∼2.5 Å is the distance between two O atoms belonging to the same PO_4 tetrahedron (the tetrahedral edge); those from the tetrahedral edges of AlO_4 and GaO_4 would occur around 2.9 and 3.0 Å, respectively. The latter two distances are superimposed on distances between pairs of atoms belonging to two different vicinal tetrahedra, corresponding to different pairs (Al−P, Ga−P, Al−O, Ga−O, and O−O pairs) that are observed above ∼2.8 Å. The distances greater than 3 Å also correspond to distances between two atoms which belong to two nonvicinal tetrahedra (medium- and long-range atomic pair distances).

Interatomic distances obtained by either Rietveld refinements or by total scattering are compared in Figure 3. The distances obtained with the two methods differ significantly particularly at high temperature. On the basis of Rietveld refinements, the Al/Ga−O and P−O distances decrease with increasing temperature, corresponding to an apparent contraction of the tetrahedra. This behavior has also been observed when standard Rietveld refinement with isotropic or anisotropic ADP's is performed on systems with a large degree of dynamic disorder.[25−28] In contrast, total scattering yields stable interatomic distances (Al−O and P−O) or an increase for the Ga−O bond that is consistent with normal thermal expansion of the tetrahedra. The Rietveld method uses the average atomic positions and average (Al, Ga) atoms to determine the "bond" length, whereas the total scattering method gives the true instantaneous atomic distances in the

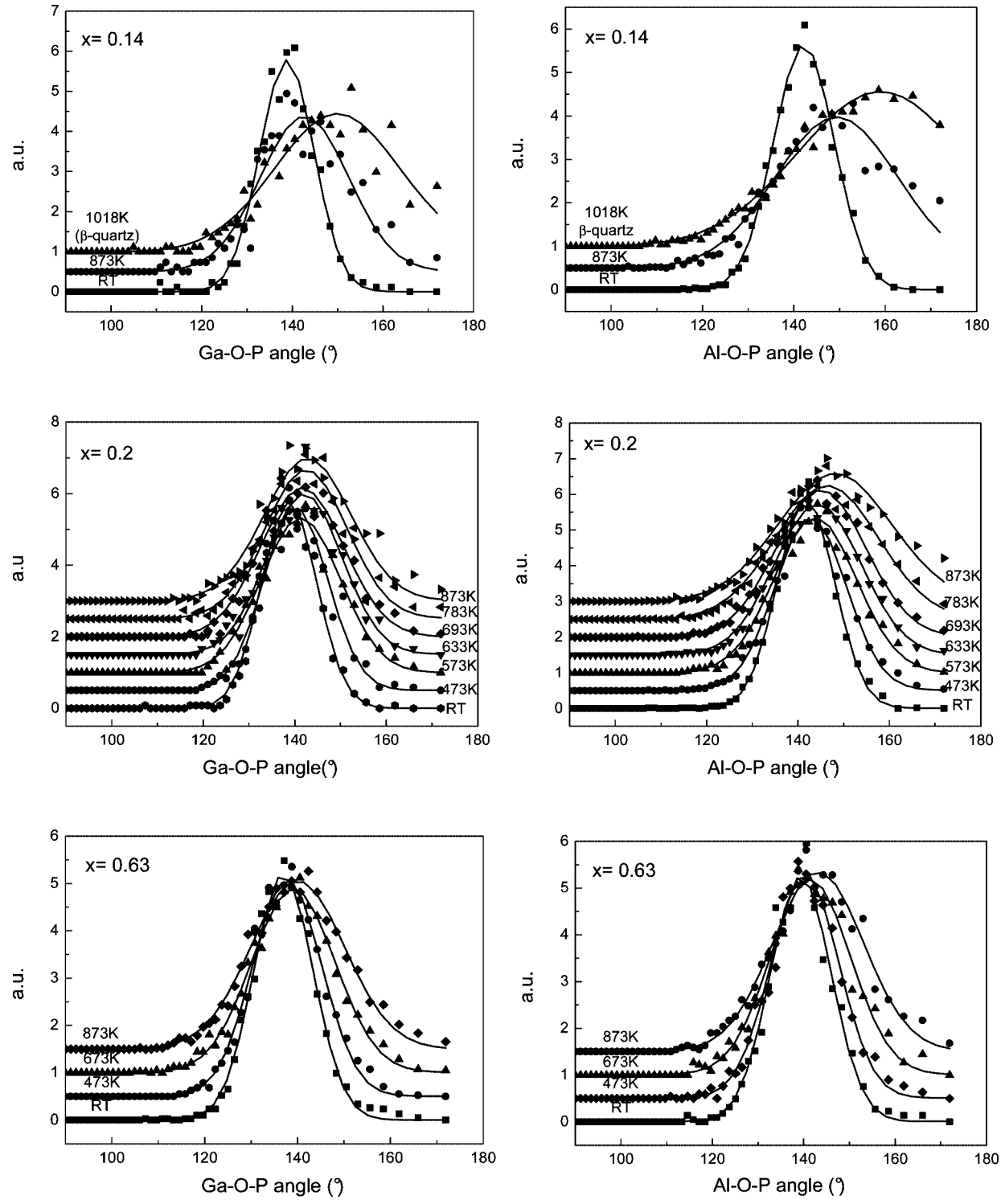

Figure 4. Ga−O−P and Al−O−P angle distributions in $Al_{(1-x)}Ga_xPO_4$ as a function of temperature.

material for each temperature and Al−O and Ga−O bonds can be distinguished.

3.3. RMC Modeling: Instantaneous Topology, Dynamic Disorder.

3.3.1. θ(Al−O−P) and θ(Ga−O−P) Angle Distributions. The experimental θ(Al−O−P) and θ(Ga−O−P) angle distributions were fitted to Gaussians (Figure 4, Table 3). At room temperature (290 K), the average values of the angles vary as a function of the composition. With increasing Ga-content, θ(Al−O−P) and θ(Ga−O−P) angles decrease corresponding to an increase in the distortion of the material (Figure 5a). The Gaussian width of the angle distribution remains sharp with a value of close to 12°. The evolution of these angles in terms of temperature differs for each composition. For the lowest Ga-content ($x = 0.14$), the θ angles increase progressively toward those found for the β-quartz type structure. At 1018 K, the (Al−O−P) and the (Ga−O−P) angle distributions become very broad and the average angle θ is 154° as found in the β-quartz structure of silica. For phosphates, values of 154.6° at 858 K and

(46) Allred, A. L.; Rochow, E. G. *J. Inorg. Nucl. Chem.* **1958**, *5*, 264.

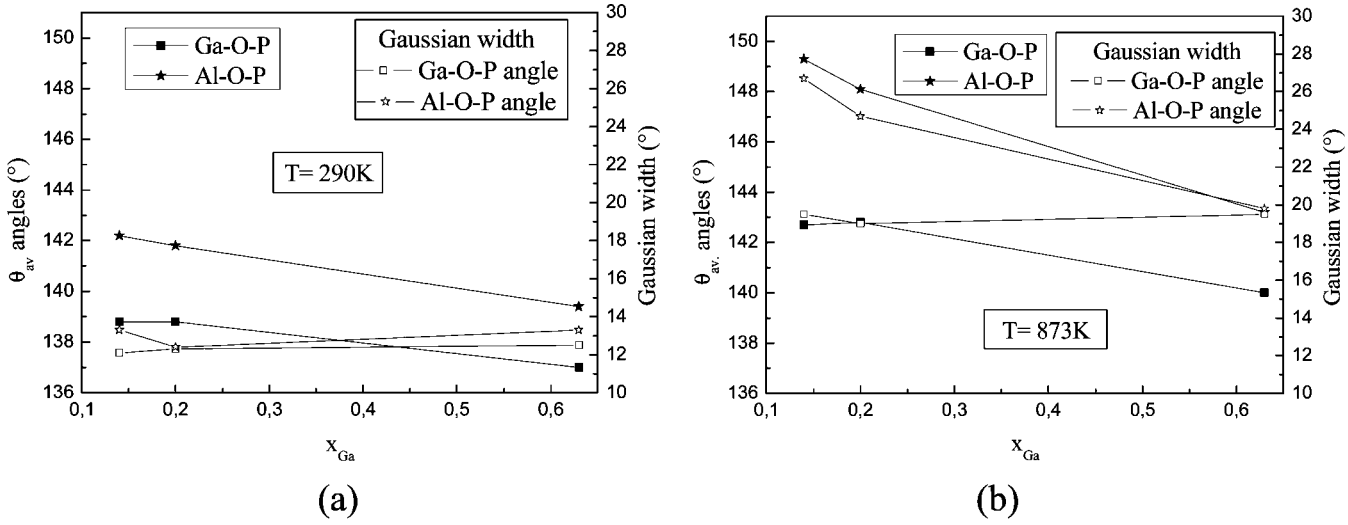

Figure 5. Average values and Gaussian width of the (Ga−O−P) and (Al−O−P) angular distributions as a function of Ga content at (a) 290 and (b) 873 K.

Table 3. Parameters of the Gaussian Fit to the Ga−O−P and Al−O−P Angle Distributions of $Al_{(1-x)}Ga_xPO_4$ as a Function of Temperature

	Ga−O−P angle		Al−O−P angle	
temperature (K)	Gaussian center	Gaussian width	Gaussian center	Gaussian width
		$x = 0.14$		
RT	138.8	12.1	142.2	13.3
873	142.7	19.5	149.3	26.7
1018	150.0	27.6	159.0	36.2
		$x = 0.2$		
RT	138.8	12.3	141.8	12.4
473	140.2	14.0	142.8	15.5
573	141.3	17.3	143.7	18.0
633	142.1	16.5	144.3	19.0
693	142.2	18.0	145.0	19.6
783	142.5	18.0	146.3	22.5
873	142.8	19.0	148.1	24.7
		$x = 0.63$		
RT	137.0	12.5	139.4	13.3
473	137.8	14.8	140.3	14.7
673	139.1	17.8	141.5	17.4
873	140.0	19.5	143.2	19.8

Table 4. Fit Parameters (average and standard deviation) of the Distribution of the Tilt Angles of GaO_4, AlO_4, and PO_4 Tetrahedra in $Al_{(1-x)}Ga_xPO_4$ as a Function of Temperature

T (K)	δ $(GaO_4)_{avg}$(deg)	std. dev.	δ $(AlO_4)_{avg}$(deg)	std. dev.	δ $(PO_4)_{avg}$ (deg)	std. dev.
			$x = 0.14$			
RT	17.6	3.6	16.8	4.2	19.5	5.4
873	15.8	7.0	11.7	9.4	14.4	10.3
1018	11.3	8.9	2.8	12.4	4.6	14.3
			$x = 0.20$			
RT	16.9	4.7	16.3	4.3	19.4	4.6
473	17.8	5.0	17.1	5.5	19.9	6.3
573	17.8	6.0	16.2	6.4	19.3	6.9
533	17.0	6.2	15.6	6.6	18.7	7.2
693	17.3	6.5	15.4	7.2	18.1	8.1
783	15.9	7.0	14.5	7.6	17.2	8.4
873	15.4	7.6	12.9	8.8	16.2	9.5
			$x = 0.63$			
RT	17.7	4.9	15.9	5.8	22.1	5.1
473	18.1	5.5	17.2	6.1	22.8	6.0
673	18.7	6.2	17.6	6.9	20.7	8.4
873	16.3	8.0	14.8	8.1	21.6	8.5

154.9° at 1005 K are found for the β-quartz-type structure of $AlPO_4$[12] and $FePO_4$,[6] respectively. At 873 K, the effect of the Ga-content is also evident (Figure 5b). The average (Ga−O−P) angle decreases from 142.7 to 140.0°, whereas the average (Al−O−P) angle decreases from 149.3 to 143.2° on increasing Ga content from $x = 0.14$ to $x = 0.63$. The Gaussian width of the (Ga−O−P) angle is largely unchanged with increasing Ga content, whereas a drastic decrease in the Gaussian width is observed for the (Al−O−P) angle. This behavior proves that the dynamic disorder decreases with increasing Ga-content. The effect of the Ga-content is clear: the presence of Ga atoms stabilizes the α-quartz structure by increasing the distortion between these two tetrahedra in the $[AlO_4]-[PO_4]$ chain.

3.3.2. Distributions of Tetrahedral Tilt Angles. Tilt angles of the three tetrahedra AlO_4, GaO_4 and PO_4 are given for $x = 0.14$ and $x = 0.63$ (Figure 6). The fit parameters (average and standard deviation, Table 4) of these distributions allow us to understand the effect of Ga content in the material. At 1018 K, for $x = 0.14$, tilt angles of AlO_4 and PO_4 have decreased drastically down to a value close to zero ($\delta = 0$ for ordered β-quartz structure), whereas the GaO_4 tetrahedra are still strongly tilted as in α-quartz-type structures. The GaO_4 tetrahedron is strongly tilted for all three compositions at all temperatures. By increasing the Ga content ($x = 0.2$ and $x = 0.63$), the AlO_4 tilt angles are more stable as a function of temperature. This effect is even more marked for the PO_4 tetrahedron. At 873 K, the GaO_4 tilt angle is quite similar (about 16°) for the three compositions. From Table 4, it is evident that the presence of GaO_4 tetrahedra (x increasing) has a greater effect on the PO_4 than the AlO_4. This can be explained by the alternation of tetrahedra in the structure. The GaO_4 tetrahedron is connected to four PO_4 tetrahedra, whereas the AlO_4 tetrahedra are present as second neighbors distributed in a statistical manner depending on x. This behavior is in agreement with the presence of decoupled AlO_4 (222 cm^{-1}) and GaO_4 (296 cm^{-1}) modes and their different temperature stabilities in Raman spectroscopy.[29] The various modes involving the PO_4 tetrahedron were found to be coupled.

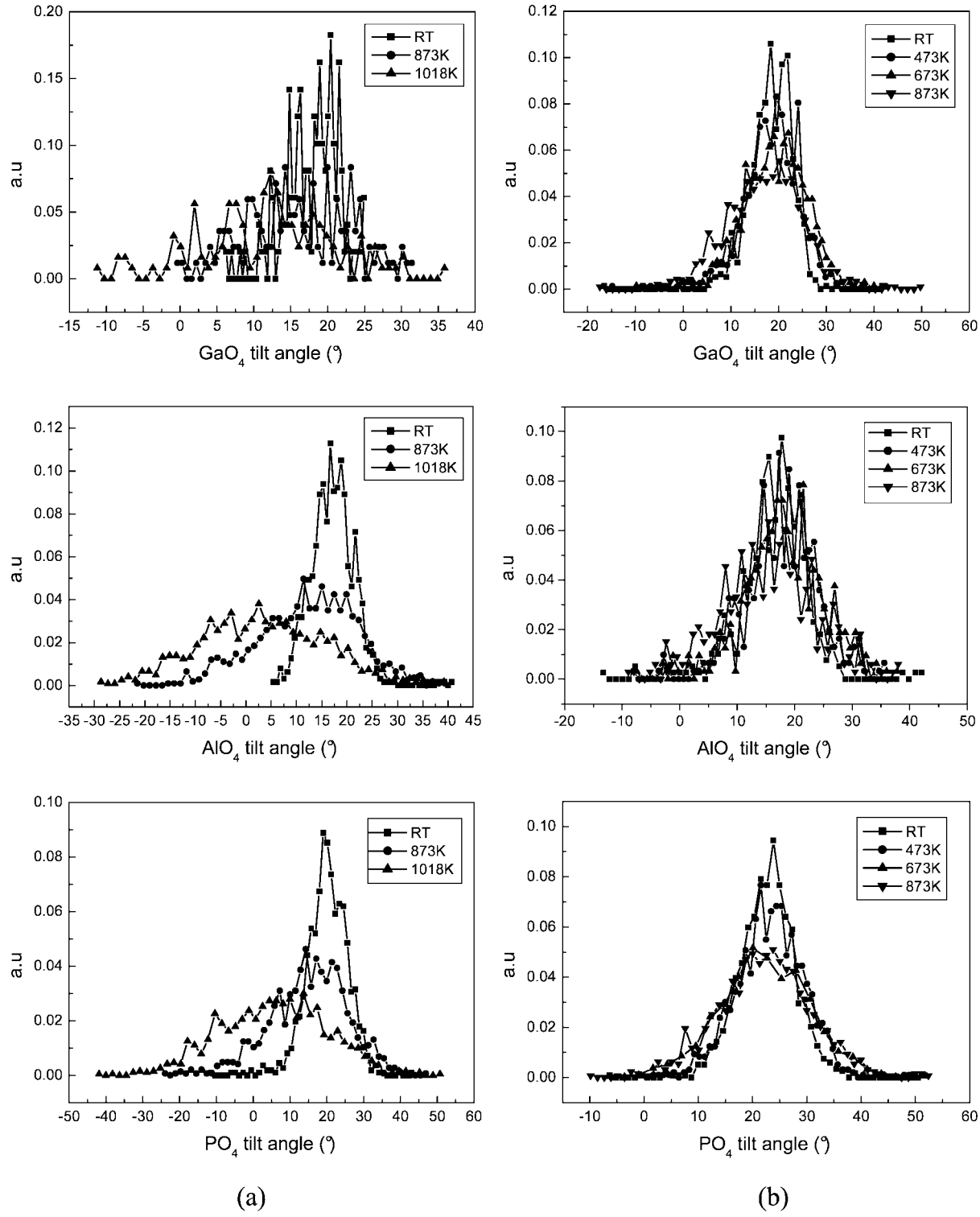

Figure 6. Tilt angles distributions of the AlO_4, GaO_4, and PO_4 tetrahedra at different temperatures for (a) $x = 0.14$ and (b) $x = 0.63$.

3.3.3. O−O−O Angles (Oxygen Sublattice). In the oxygen sublattice (Figures 7), the O−O−O angles are well defined at room temperature, with clearly identifiable intertetrahedral peaks in the distributions. For the lowest Ga content ($x = 0.14$), a high degree of dynamic disorder akin to that found for the β-quartz[25] structure appears at 873 K (i.e., the intertetrahedral distribution becomes largely featureless). In the case of the highest Ga content ($x = 0.63$), the O−O−O angle distribution is still well-defined at 873 K. This shows that the dynamic disorder decreases with increasing Ga content. These two types of behavior are in agreement with the previous results obtained by neutron total scattering for SiO_2[25] and $GaPO_4$.[28] For SiO_2, the dynamic disorder observed in the oxygen sublattice well before the α-β transition (above 573 K) is the origin of the loss of the piezoelectric properties.[26,27] For $GaPO_4$, this phenomenon only begins above 1023 K, thus $GaPO_4$ may be a useful material for high-temperature applications.

The Ga content has two consequences on the behavior of the material: it stabilizes the α-quartz structure and it

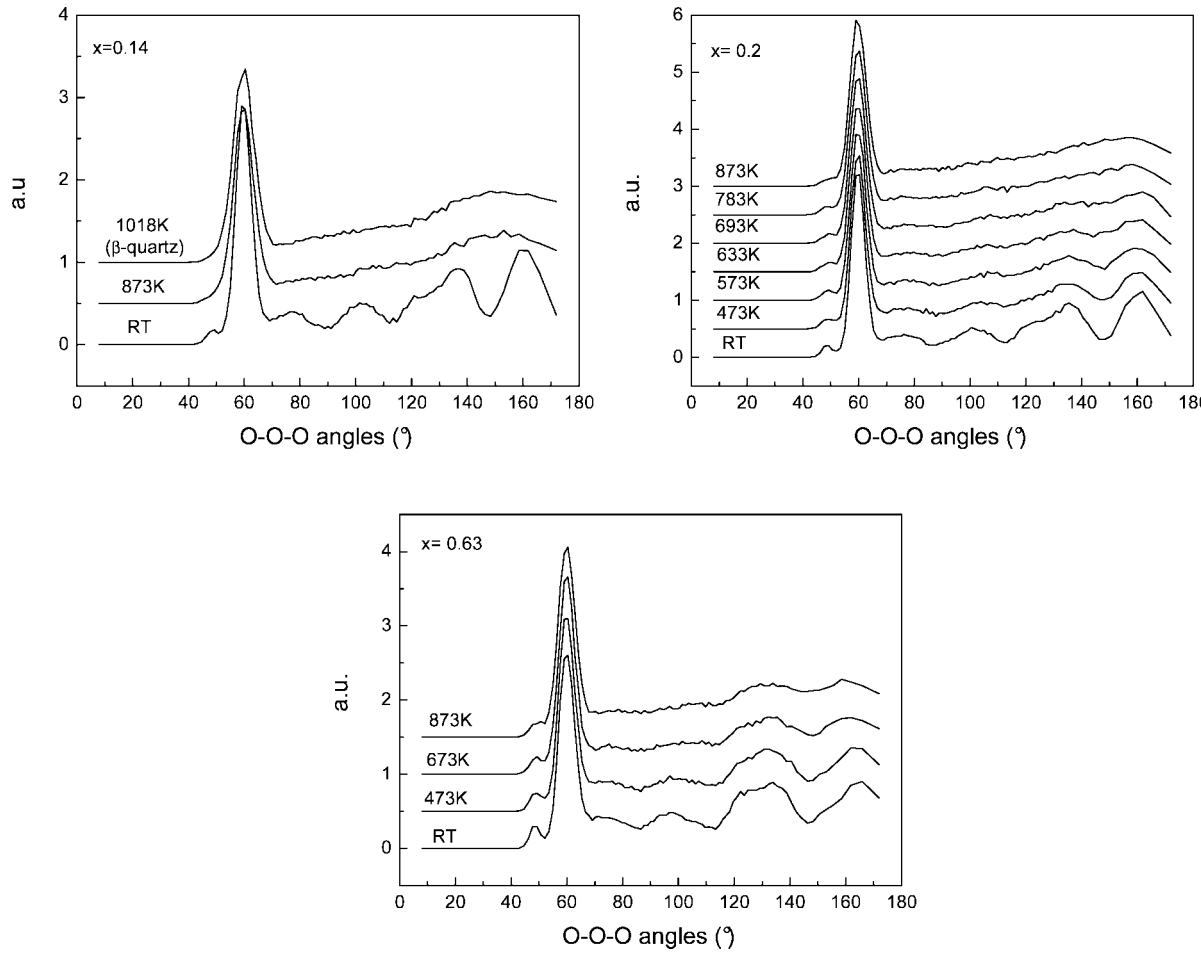

Figure 7. O−O−O angle distributions in $Al_{(1-x)}Ga_xPO_4$ as a function of temperature. Note that the strong peak centered at 60° corresponds to intratetrahedral angles; all other features correspond to intertetrahedral angles with some additional contributions from nonvicinal triplets.

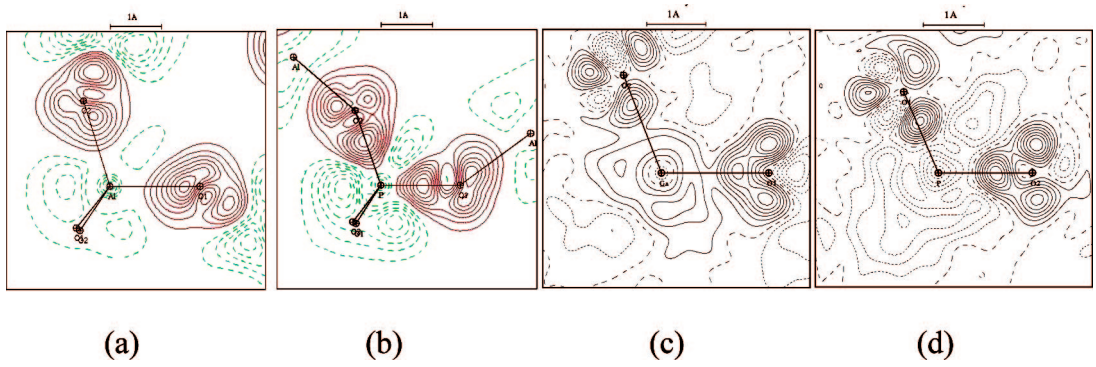

Figure 8. Model dynamic deformation maps for (a, b) $AlPO_4$ and (c, d) $GaPO_4$ from high-resolution XRD. Positive contours of 0.05 ($AlPO_4$) and 0.1 e/Å^3 ($GaPO_4$) are represented by continuous lines.

decreases the dynamic disorder in the oxygen sublattice. These results illustrate very clearly the influence of chemical composition and the interest of the solid solutions such $Al_{1-x}Ga_xPO_4$ for tuning the piezoelectric properties by varying the chemical composition (x).

3.4. Origin of the Enhanced Stability of the α-Quartz-Type Phase in Ga-Rich Compositions. The degree of covalent bonding is a function of the nature of the participating atoms (radius, charge, electronegativity, etc.). Indeed, when the bonds are more covalent, they have a more marked directional behavior with higher electron density between the two atoms that increases the stability of the structure. In our case, we consider the atomic electronegativity χ given by Allred−Rochow,[46] taking into account the effective nuclear charge Z^* including the Slater effect of the valence electrons. These values of electronegativity better describe the polarization effect of the bonds and are more useful for describing the physical properties of materials. For the $Al_{(1-x)}Ga_xPO_4$ solid solution, the values of the different atoms are χ(Al) = 1.47, χ(Ga) = 1.82, χ(P) = 2.06, and χ(O) = 3.50. In the GaO_4 tetrahedron, the difference in electronegativity $\Delta\chi = \chi(O) - \chi(Ga) = 1.68$. For the AlO_4 tetrahedron, the same calculation gives $\Delta\chi = 2.03$; the Ga−O bond is more covalent than the Al−O bond. This result has

been confirmed by the partial charges in $GaPO_4$ and $AlPO_4$, which have been calculated from the analysis of the electronic charge densities determined based on Bader's method[44] using high-resolution X-ray diffraction. The more covalent character of P, compared to Ga, and even more Al, shows up in these $\Delta\rho_{dyn}$ maps where the accumulation of electron density is significantly greater in P−O bond than in other bonds (Figure 8). The partial charges obtained for the different atoms are: Ga(+0.63), O(−1.12/−1.13), P(+2.3) for $GaPO_4$ and Al(+2.3), O(−1.45/−1.47), P(+3.4) for $AlPO_4$, reflecting al the more ionic character of the Al−O bond in $AlPO_4$ than the Ga−O bond in $GaPO_4$.

Moreover, the Ga atom is larger than the Al atom, which closes the intertetrahedral angle θ (increases the distortion). The size and the electronic configuration of Ga ([Ar] $3d^{10}4s^24p^1$) give rise to more covalent bonding with the oxygen atoms, which reduces the dynamic disorder at high temperature.

This study demonstrates the role of the cation sublattice and the chemical composition on the material's behavior, increasing its thermal stability and reducing dynamic disorder with increasing Ga content. This result is in agreement with the concept of "pseudoatoms and preferred skeletons in crystals" developed by A.Vegas,[47] which considers that the crystal structures and consequently oxygen positions are imposed by the "cations" of the p-block.

From these results, it is possible to relate the degree of bond covalency to the structural and piezoelectric properties of the materials. Indeed, by incorporating larger and more polarizable atoms, like Ga, in the lattice, the structural distortion increases with the covalency of the bond as confirmed by the partial charges measured from atomic density maps. The bond is therefore more polarizable and piezoelectric properties are thus increased. The piezoelectric effect in α-quartz homeotypes is not a simple displacement of ionic charges and the polarization of the electronic environment around the atoms plays a major role. The improvement in piezoelectric properties is clear going from $AlPO_4$ ($k = 11\%$) to $GaPO_4$ ($k = 16\%$), whereas in the same time, the ionic charge decreases as found in the present study and the strength of the covalent bond increases. This clearly shows the contribution of the bond polarizability.

(47) Vegas, A.; Garcia-Baonza, V. *Acta Crystallogr., Sect. B* **2007**, *63*, 339.

4. Conclusion

The current results demonstrate the link that can be made between the materials chemistry and physical properties by using powerful investigation tools like total neutron scattering coupled with computer modeling (RMC). In the $Al_{(1-x)}Ga_xPO_4$ solid solution, it is shown that by increasing the Ga content, the thermal stability of the α-quartz phase increases whereas the dynamic disorder is reduced. The evolution of instantaneous structure demonstrated that the presence of GaO_4 tetrahedra imposes the tilt angles of the AlO_4 and PO_4 tetrahedra and consequently determines the thermal stability of the material. These results are due to the presence of Ga atoms in the structure, which enhance the covalent behavior of the bond with a corresponding increase in the electron density between the atoms. The increased size of the Ga atoms results in the closing of the θ(Al−O−P and Ga−O−P) angles thus improving the piezoelectric properties of the material. This approach may be applied to other materials with the aim of improving their thermal stability by chemical substitution through enhancing the covalent nature of their chemical bonds.

Acknowledgment. We thank the TMR program of the European Union for financing the total neutron scattering experiments at ISIS.

Supporting Information Available: Final Rietveld refinements fits for all the structures and the anisotropic thermal parameters for the various atoms (PDF and text files). This material is available free of charge via the Internet at http://pubs.acs.org.

CM801667P